

# Luttinger liquid properties of the steady state after a quantum quench

D.M. Kennes and V. Meden

*Institut für Theorie der Statistischen Physik, RWTH Aachen University and  
JARA—Fundamentals of Future Information Technology, 52056 Aachen, Germany*

(Dated: August 16, 2018)

We study the dynamics resulting out of an abrupt change of the two-particle interaction in two models of closed one-dimensional Fermi systems: (a) the field theoretical Tomonaga-Luttinger model and (b) a microscopic lattice model. Using a nonperturbative approach which is controlled for small two-particle interactions we are able to reach large times allowing us to access the properties of the steady state of the lattice model. Comparing those to the exact solution of the full dynamics in the Tomonaga-Luttinger model we provide evidence for universal Luttinger liquid behavior.

PACS numbers: 71.10.Pm, 02.30.Ik, 03.75.Ss, 05.70.Ln

## I. INTRODUCTION

With the rapid progress in the preparation and measurement techniques for isolated cold gases<sup>1</sup> investigating the fundamental questions of if and how a closed quantum many-body system prepared in a nonequilibrium initial state approaches a stationary one is within experimental reach. Studying the physics of the steady state itself is of particular interest if it is nonthermal,<sup>2</sup> that is expectation values of observables differ from those computed using a canonical statistical operator with the temperature fixed by the excess energy. One-dimensional (1d) interacting Fermi systems are promising candidates for realizing such unusual nonequilibrium states as in many of those the dynamics is restricted not only by energy conservation but by additional conservation laws.<sup>3</sup> An often studied protocol, which we also employ, is an abrupt quench of the amplitude  $U$  of the two-particle interaction: the system is prepared in the canonical ensemble of an initial Hamiltonian  $H(U_i)$ , while the time evolution is performed with  $H(U_f)$ ,  $U_f \neq U_i$ . After taking the thermodynamic limit local observables might become stationary at long times  $t \rightarrow \infty$ .<sup>4,5</sup>

In equilibrium the exactly solvable Tomonaga-Luttinger (TL) model<sup>6,7</sup> is the infrared fixed point model under a renormalization group (RG) flow of a large class of interacting 1d models in their ungapped metallic phase.<sup>9</sup> The low-energy physics of models out of this Luttinger liquid (LL) universality class<sup>8</sup> is given by that of the TL model. For spinless models the fixed point is characterized by the velocity  $v$  of the elementary excitations and the LL parameter  $K$  entering exponents of algebraically decaying correlation functions. Both depend on the parameters of a given model, in particular on  $U$ .

One of the hallmarks of LLs is their sensitivity towards inhomogeneities. For repulsive interactions with  $K < 1$  the ground state density response function of a LL diverges as<sup>10</sup>  $\chi(q, \omega = 0) \sim |q - 2k_F|^{2K-2}$ , with the Fermi momentum  $k_F$ , indicating that even a single weak impurity acts as a strong perturbation. The homogeneous perfect chain fixed point is unstable.<sup>11-13</sup> The system flows towards an open chain one with strong

consequences for the equilibrium low-energy properties; e.g. the linear conductance vanishes as  $G \sim T^{2K-1-2}$  for temperature  $T \rightarrow 0$ .

We provide evidence that the steady state of a microscopic 1d lattice model after an interaction quench is characterized by the same power laws as found in the steady state of the TL model after a similar quench<sup>14-19</sup> with the  $K$  taken for the considered model parameters. As the RG arguments leading to this type of LL universality in equilibrium<sup>9</sup> cannot directly be transferred to nonequilibrium<sup>16,19-22</sup> this finding is far from obvious. It complements earlier indications of LL universality in the time evolution towards the steady state.<sup>23</sup> We compute the time evolution of the density as a function of the distance from an open boundary as well as that of the conductance across a single impurity as a function of  $T$  and take  $t \rightarrow \infty$ . The dynamics of the TL model is solved exactly using standard bosonization.<sup>6,7,24</sup> To study the time evolution of the lattice model we use an approximate functional RG<sup>25</sup> based approach which so far was only applied to open quantum systems.<sup>26</sup> For small two-particle interactions this technique allows controlled access to time scales large enough such that the physics is dominated by the steady state. It complements calculations using the density-matrix renormalization group (DMRG) which provide ‘exact’ results at small  $t$  but abruptly become unreliable beyond a characteristic time scale;<sup>27-30</sup> the latter might be smaller than the one on which the steady state is reached.<sup>23</sup> We show that the fixed point structure of a single impurity in a nonequilibrium steady-state LL is similar to the one in equilibrium.<sup>11</sup>

The rest of the paper is structured as follows. In the following section we discuss the exact solution of the quench dynamics of the TL model via bosonization. In Sect. III we introduce the lattice model considered and show how its relaxation dynamics can be treated approximately within the functional RG. We then compare the prediction of the TL model for observables and correlation functions of the steady state with results obtained for the lattice model. Finally, in Sect. IV we briefly discuss the relation of our results to those obtained by field-theoretical methods and hint towards open questions.

## II. TOMONAGA-LUTTINGER MODEL

The starting point of our investigation of LL universality is the exact computation of the desired observables and correlation functions within the (spinless) TL model. Starting out from the 1d electron gas the TL model is obtained by linearizing the single-particle dispersion and keeping only the marginal two-particle scattering terms. In contrast to earlier studies on interaction quenches in the TL model<sup>14–20,23,31–33</sup> we consider the one with open boundaries at  $x = 0$  and  $x = L$ .<sup>11,34</sup> This allows us to distinguish between bulk and boundary LL exponents.<sup>35,36</sup> While in equilibrium the former are quadratic in the two-particle interaction the latter are linear. The model is given by

$$H_{\text{TL}} = \sum_{n=1}^{\infty} k_n \left[ v_{\text{F}} b_n^{\dagger} b_n + \frac{1}{4\pi} u(k_n) (b_n^{\dagger} + b_n)^2 \right], \quad (1)$$

with the Fermi velocity  $v_{\text{F}}$ ,  $k_n = n\pi/L$ , the two-particle potential  $u(k)$ , and bosonic operators  $b_n^{(\dagger)}$  associated with the density of the fermions. Employing a Bogoliubov transformation  $H_{\text{TL}}$  can be written as a diagonal quadratic form in eigenmodes with (bosonic) ladder operators  $\alpha_n^{(\dagger)}$  and energy  $\omega_n = v_{\text{F}} k_n \sqrt{1 + u(k_n)/(\pi v_{\text{F}})}$ . To keep the formulas transparent we here take the noninteracting canonical statistical operator  $\rho_c^0 = \exp[-\beta H_{\text{TL}}(u=0)] / \text{Tr}\{\exp[-\beta H_{\text{TL}}(u=0)]\}$  as the initial state with  $\beta = T^{-1}$ ; in Appendix A we describe the changes when starting in the canonical state with  $u_i(k) > 0$ .

Using the Bogoliubov transformation and standard bosonization of the field operator<sup>6,7,24,34</sup> it is straight forward to derive closed analytical expressions for the density  $n_t(x)$ , with  $x$  being the distance from the boundary, the density of states (DOS)  $\rho_t(\omega)$ , and the density response  $\chi_t(q, \omega)$  (see Appendix A). The latter two functions can be used to compute the conductance in the limits of small and large impurities (see below). The expectation values are obtained by taking  $\text{Tr}[\rho_c^0 e^{iHt} O e^{-iHt}]$ , where  $O$  stands either for an observable or the operator product defining a correlation function. After performing the thermodynamic limit the steady state values follow by taking  $t \rightarrow \infty$ ; all the above quantities converge and their steady-state limits are indicated by dropping the index  $t$ . We verified that the same  $t \rightarrow \infty$  expectation values can be computed using the statistical operator of a generalized Gibbs ensemble (GGE).<sup>3,14,16,17,19,37</sup>

At  $T = 0$ , with the initial state given by the noninteracting ground state, the steady state reached after the quench is ‘critical’, that is characterized by power-law scaling.<sup>14–16,19</sup> As a consequence different observables show characteristic power-law behavior with exponents which in general are different to the exponents found in equilibrium.<sup>6–11</sup> They can all be expressed in terms of the models LL parameter  $K = [1 + u(0)/(\pi v_{\text{F}})]^{-1/2}$  after the quench. The access density  $\Delta n(x) = n(x) - \nu$ , where  $\nu$  denotes the filling, for large distances from the boundary

observable/correl. funct.	variable	eq. exp.	steady-state exp.
access density $\Delta n$	$x$	$-K$	$-(K^2 + 1)/2$
local DOS $\rho$	$\omega$	$K^{-1} - 1$	$(K^{-2} - 1)/2$
bulk $\chi$ at $\omega = 0$	$q - 2k_{\text{F}}$	$2(K - 1)$	$K^2 - 1$

TABLE I. Equilibrium and steady-state scaling exponents.

$x$  falls off as

$$\Delta n^{\text{eq}}(x) \sim x^{-K} \sin(2k_{\text{F}}x) \quad (2)$$

$$\Delta n^{\text{st}}(x) \sim x^{-(K^2+1)/2} \sin(2k_{\text{F}}x) \quad (3)$$

where superscripts eq and st refer to the ( $T = 0$ ) equilibrium or the steady state reached after the interaction quench, respectively. Both cases show damped Friedel oscillations with frequency  $2k_{\text{F}}$ . One finds that as the (repulsive) interaction strength is increased and thus  $K$  becomes smaller (starting at  $K = 1$  for the noninteracting case), the access density in the presence of a boundary in both cases falls off slower than for vanishing two-particle interaction, but with different exponents. The difference between ground- and steady-state exponents in the TL model was emphasized before considering other observables and correlation functions.<sup>14–16,19</sup>

Additionally, we consider the frequency resolved local DOS  $\rho(\omega)$  at small  $|\omega|$  and close to the boundary. In the ground state it is suppressed as

$$\rho^{\text{eq}}(\omega) \sim |\omega|^{K^{-1}-1}, \quad (4)$$

which changes to

$$\rho^{\text{st}}(\omega) - \rho^{\text{st}}(0) \sim |\omega|^{(K^{-2}-1)/2} \quad (5)$$

in the nonequilibrium steady state. In contrast to the equilibrium case in the steady state reached after the interaction quench the DOS takes a finite value  $\rho^{\text{st}}(0)$  at  $\omega = 0$ .<sup>38</sup> This incomplete suppression is reminiscent of the equilibrium DOS at finite temperatures for which the zero frequency value scales as  $T^{K^{-1}-1}$ .<sup>35</sup> The exponents of the power law behavior with which the  $\omega = 0$  spectral weights are reached differ between the equilibrium and steady-state situation. Both increase with increasing interaction.

Finally, we compute the zero frequency bulk charge susceptibility  $\chi(\omega = 0)$  for wave vectors close to the backscattering condition  $q = 2k_{\text{F}}$ . The divergence ( $K < 1$  for repulsive interactions) changes from the ground-state result

$$\chi^{\text{eq}}(\omega = 0, q - 2k_{\text{F}}) \sim (q - 2k_{\text{F}})^{2(K-1)} \quad (6)$$

to

$$\chi^{\text{st}}(\omega = 0, q - 2k_{\text{F}}) \sim (q - 2k_{\text{F}})^{K^2-1} \quad (7)$$

in the steady state. The comparison of the equilibrium and steady state exponents is summarized in Table I.

In the next section we directly compare the decay of the densities Friedel oscillations off the boundary in the steady state of a microscopic lattice model with the TL model prediction.

The scaling behavior of the bulk static density response  $\chi^{\text{st}}(q, \omega = 0)$  allows us to make predictions for how the steady state reacts to a single impurity. For repulsive interactions  $K^2 - 1 < 0$  and  $\chi$  diverges for  $q \rightarrow 2k_{\text{F}}$ . As in equilibrium even a weak single impurity strongly disturbs the homogenous system. When applying an infinitesimal bias voltage  $V$  across the impurity the steady-state linear conductance  $G = dI^{\text{st}}/dV$  (with the stationary current  $I^{\text{st}}$ ) is expected to scale as  $G_0 - G(T) \sim T^{K^2-1}$ , with the constant homogenous chain conductance  $G_0$ . The power law holds as long as the right hand side stays small, that is for not too small  $T$ . Using the language of equilibrium RG this indicates that the perfect chain fixed point is unstable. In contrast, the steady-state analog of the open chain one is stable as follows from the scaling of the local DOS. Fermis Golden Rule-like arguments lead to a tunneling conductance across a weak link connecting two semi-infinite chains which scales as  $G \sim T^{K^2-1}$  in a temperature regime which at the lower end is cut off by the finite DOS at  $\omega = 0$  [see Eq. (5)]. These arguments do not rule out intermediate impurity fixed points. Provided the concept of LL universality holds for the steady state we expect to find those weak and strong impurity scaling laws of  $G(T)$  for a lattice model with the  $K$  of the model considered.

### III. MICROSCOPIC MODEL

We consider the lattice model of spinless fermions with nearest-neighbor hopping  $J$  as well as interaction  $U$  and open boundaries terminating the  $N$ -site chain given by

$$H_{\text{LM}}(U) = \sum_{j=1}^{N-1} \left[ -Jc_j^\dagger c_{j+1} + \text{H.c.} + Uc_j^\dagger c_j c_{j+1}^\dagger c_{j+1} \right] \quad (8)$$

in standard second quantized notation. In equilibrium the model is (A) Bethe ansatz solvable and (B) shows universal LL physics with  $K$  and  $v$  exactly known.<sup>8</sup> It is commonly believed that because of (A) the steady state after an interaction quench is described by a GGE but the corresponding statistical operator was so far neither constructed nor was a proof of its existence given. Our analysis does not rely on any such assumption. When discussing the impurity physics  $H_{\text{LM}}$  is supplemented by a hopping impurity  $H_{\text{imp}} = hc_{N/2}^\dagger c_{N/2+1} + \text{H.c.}$  of strength  $h \in [0, J]$  located in the middle of the chain.

#### A. Method

To compute the time evolution of the density  $n_j$  as well as the conductance  $G$  we use an approximate functional

RG<sup>25,26</sup> based approach. Here, we employ the lowest order truncation scheme in the two-particle interaction. To this order the self-energy acquires a RG flow, which is crucial to capture the impurity physics,<sup>11-13</sup> while the two-particle vertex remains the bare one. Renormalization of the latter is a higher order effect. The same truncation level was earlier shown to capture the equilibrium LL properties of inhomogeneous lattice models including the characteristic power-law scaling, with exponents agreeing to the exact ones to leading order in  $U$ .<sup>12,13</sup> Motivated by the functional RG's success in describing the equilibrium properties of inhomogeneous lattice models, we extend it to tackle the quench dynamics in such systems. As the functional RG can directly be applied to the microscopic model, i.e. without the need of mapping it to an effective low-energy field-theory, the information about the high energy modes is not lost and one can hope to find reliable results also for the relaxation at short times (being influenced by the high energy characteristics of the underlying lattice model) as well as the crossover behaviour. We study the relaxation dynamics and the steady state of a closed many-body system described by a lattice model of spinless fermions with nearest neighbor hopping and interaction. Compared to the functional RG approach to time evolution for open quantum systems introduced in Ref. 26, some minor amendments need to be made. Those are outlined next.

We can treat Hamiltonians of the form

$$H = H_0 + H_{\text{int}}, \quad (9)$$

$$H_0 = \sum_{ij} \epsilon_{ij} c_i^\dagger c_j, \quad (10)$$

$$H_{\text{int}} = \frac{1}{4} \sum_{ijkl} \bar{u}_{ijkl} c_i^\dagger c_j^\dagger c_l c_k \quad (11)$$

written in standard second quantization. Here  $\bar{u}_{ijkl}$  is the antisymmetrized two-particle interaction. For our lattice model  $H_0 = H_{\text{LM}}(U = 0)$  and  $H_{\text{int}} = \sum_{j=1}^{N-1} Uc_j^\dagger c_j c_{j+1}^\dagger c_{j+1}$ . The indices  $i, j, \dots$  stand for the quantum numbers, e.g. the  $N$  Wannier states in our lattice model. We assume an initial density matrix

$$\rho^0 = \frac{e^{\sum_{ij} \beta_{ij} c_i^\dagger c_j}}{\text{Tr} \left[ e^{\sum_{ij} \beta_{ij} c_i^\dagger c_j} \right]} \quad (12)$$

which allows for the application of Wick's theorem. For our calculations we always choose the noninteracting canonical statistical operator  $\rho^0 = \rho_c^0 = \exp(-\beta H_0) / \text{Tr}[\exp(-\beta H_0)]$ . We introduce a cutoff in the noninteracting Keldysh<sup>39</sup> Green functions  $g$  (as motivated in Ref. 26) by considering

$$g^{\text{ret}, \Lambda}(t, t') = -i\Theta(t - t')e^{-i\epsilon(t-t')}e^{-i\Lambda(t-t')} \quad (13)$$

$$= [g^{\text{adv}, \Lambda}(t', t)]^\dagger, \quad (14)$$

$$g^{\text{K}, \Lambda}(t, t') = -ig^{\text{ret}, \Lambda}(t, 0)(1 - 2\bar{n})g^{\text{adv}, \Lambda}(0, t'), \quad (15)$$

with  $\epsilon$  being the  $N \times N$  matrix with entries  $\epsilon_{ij}$  and  $\bar{n}_{ii'} = \text{Tr} [\rho^0 d_{i'}^\dagger d_i]$ . The self-energy is obtained by solving a set of coupled differential flow equations

$$\begin{aligned} \partial_\Lambda \Sigma_{i_1 i_1'}^{\text{ret}, \Lambda}(t', t) &= \partial_\Lambda \Sigma_{i_1 i_1'}^{\text{adv}, \Lambda}(t', t) \\ &= - \sum_{i_2, i_2'} S_{i_2' i_2}^{\text{K}, \Lambda}(t, t) (-i \bar{u}_{i_1 i_2 i_2' i_1'}(t)) \delta(t' - t), \end{aligned} \quad (16)$$

$$\partial_\Lambda \Sigma^{\text{K}, \Lambda} = 0, \quad (17)$$

with the initial conditions at  $\Lambda = \infty$

$$\Sigma_{i' i}^{\text{ret}, \Lambda = \infty}(t', t) = \frac{1}{2} \delta(t - t') \sum_j \bar{u}_{i' j i j}, \quad (18)$$

$$\Sigma_{i' i}^{\text{K}, \Lambda = \infty}(t', t) = 0. \quad (19)$$

The right hand sides of the flow equations contain

$$S^{\text{K}, \Lambda} = \partial_\Lambda^* G^{\text{K}, \Lambda}, \quad (20)$$

with the full cutoff dependent Keldysh component of the Green function

$$G^{\text{K}, \Lambda}(t, t') = -i G^{\text{ret}, \Lambda}(t, 0) (1 - 2\bar{n}) G^{\text{adv}, \Lambda}(0, t'). \quad (21)$$

The star differential operator  $\partial_\Lambda^*$  acts only on the free Green function  $g^{\text{ret}/\text{adv}, \Lambda}$ , not on  $\Sigma^\Lambda$ , in the Dyson series expansion  $G^{\text{ret}/\text{adv}, \Lambda} = g^{\text{ret}/\text{adv}, \Lambda} + g^{\text{ret}/\text{adv}, \Lambda} \Sigma^\Lambda g^{\text{ret}/\text{adv}, \Lambda} + \dots$  used to calculate  $G^{\text{ret}/\text{adv}, \Lambda}$ . An approximation to the self-energy of the cutoff-free problem is obtained at  $\Lambda = 0$ . How to efficiently evaluate Eq. (21) is summarized in Appendix B.

An approximation for the occupancy of site  $j$  can directly be obtained from the Keldysh Green function at the end of the RG flow as

$$n_j(t) = \frac{1}{2} - \frac{i}{2} G_{jj}^{\text{K}, \Lambda=0}(t, t). \quad (22)$$

To calculate the current flowing from the left to the right half of the lattice in our microscopic model of interacting spinless fermions, we need to determine

$$I(t) = -\frac{d}{dt} \langle N_L(t) \rangle_{\rho^0}, \quad (23)$$

where  $N_L$  is defined as  $N_L(t) = \sum_{j=1}^{N/2} n_j(t)$ , with  $n_j = c_j^\dagger c_j$  being the occupancy operator of site  $j$  and  $\langle \dots \rangle_{\rho^0}$  denotes the expectation value with respect to  $\rho^0$ .<sup>40</sup> For simplicity we assume an even number of lattice sites  $N$ . Furthermore, we use

$$I(t) = -i \langle [H, N_L](t) \rangle_{\rho^0} = (h - J) G_{N/2N/2+1}^<(t, t) + \text{c.c.} \quad (24)$$

with  $G_{N/2N/2+1}^<(t, t)$  being the equal-time lesser Green function of the interacting system.<sup>39</sup> The functional RG method used here provides an approximation for this given by

$$G_{ij}^<, \Lambda=0(t, t) = \frac{1}{2} \left[ i - G_{ij}^{\text{K}, \Lambda=0}(t, t) \right]. \quad (25)$$

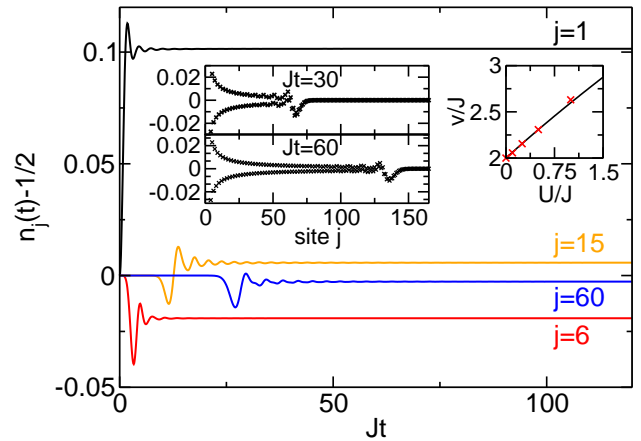


FIG. 1. (Color online) Functional RG data for the time evolution of  $n_j(t) - \nu$  at half filling  $\nu = 1/2$  after a quench in the interaction amplitude from  $U/J = 0$  to  $U/J = 0.5$  for  $N = 10^3$ ,  $T = 0$ , and different sites  $j$ . Left inset: Friedel oscillations induced by the boundary and the propagation of a main signal from the boundary to  $j \approx vt$  for two values of  $t$ . Right inset: Velocity of the main signal for different  $U$  (symbols). The exact Bethe ansatz  $v$  (line) is in excellent agreement with our data.

Therefore, plugging this lesser Green function into Eq. (24) allows to compute an approximation to the current and from this the conductance by numerical differentiation.

## B. Results

In Fig. 1 we show the access density  $n_j(t) - \nu$ , with the filling  $\nu$ , for fixed  $j$  starting out of the noninteracting impurity free ground state ( $T = 0$ ). We can reach times of the order of a few  $10^2/J$  which has to be contrasted to the DMRG approach which becomes unreliable for times of the order of  $10/J$ .<sup>23</sup> As shown in the main plot and the left inset a signal originating from the left boundary travels through the system. A similar one is generated at the right one. For a spatial region in which the left signal passed through and the right one did not enter yet the density becomes stationary. The physics for  $t \approx 10^2/J$  and  $j$  up to  $\mathcal{O}(10^2)$  is thus dominated by the steady state and does barely suffer from finite size effects. The two signals propagate with the LL velocity  $v$ ,<sup>41–43</sup> with our method providing an excellent approximation to the exact  $v$  (right inset of Fig. 1).

In Fig. 2 we compare the functional RG data to numerically exact DMRG results for the time evolution after a quench in the interaction amplitude from  $U/J = 0$  to  $U/J = 0.2$ . This value of  $U$  is of the same order as taken for all further analysis. On the scale of the plot the two datasets are indistinguishable for all sites  $j$  and all times reachable with DMRG.<sup>27–30</sup> Within our DMRG approach to prepare the noninteracting ground state an iterative single site algorithm in matrix product state formula-



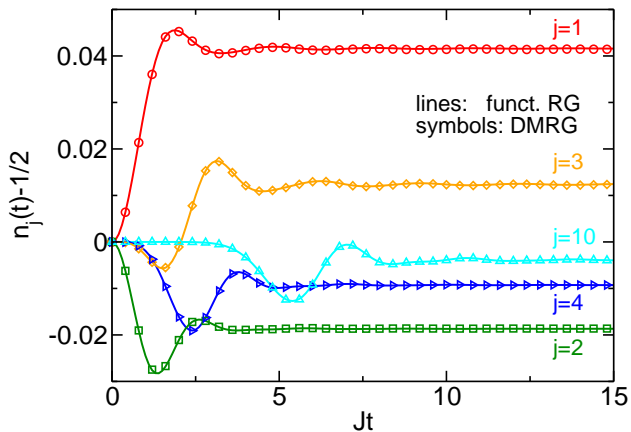


FIG. 2. (Color online) Comparison of functional RG and DMRG data for the time evolution of  $n_j(t) - \nu$  at half filling  $\nu = 1/2$  after a quench in the interaction amplitude from  $U/J = 0$  to  $U/J = 0.2$  for  $N = 10^2$ ,  $T = 0$ , and different sites  $j$ . Functional RG and the numerically exact DMRG are in excellent agreement for times reachable by the DMRG calculation.

tion was employed. The resulting wavefunction was then subjected to a real time evolution using a fourth order Suzuki-Trotter decomposition ( $J\Delta t = 0.2$ ) ensuring that the discarded weight stays below a certain  $\epsilon$  (different  $\epsilon$  ranging from  $10^{-5}$  to  $10^{-8}$  were tested to yield coinciding results). The technical details are described in length in Ref. 27. The excellent agreement of the results obtained by both methods does not only strengthen our confidence in the functional RG approach for the following steady state analysis, but also shows that indeed within functional RG we correctly incorporate also the high energy physics of the underlying lattice model, which is crucial for short times. The numerically exact solution of the time evolution within DMRG can however not be pushed to times large enough to allow for the sensitive analysis of power-law scaling conducted in the following with our functional RG approach.

In analogy to the ground state density<sup>12</sup> the stationary one  $n_j^{\text{st}}$  shows Friedel oscillations with frequency  $2k_F$  (see the  $j < 80$  region of the lower part of the left inset of Fig. 1). We next analyze their decay. Figure 3 shows the log-derivative of  $|n_j^{\text{st}} - 1/2|$ , that is an effective exponent. The dashed lines is the prediction from the TL model of Table I with the exact lattice model  $K$ . Our data are consistent with a power-law decay and the TL model exponent. This finding is our first indication of LL universality of the steady state. The differences between the exact exponent and our result is of order  $(U/J)^2$ . On the right hand side of our RG flow equations we do not fully capture terms  $\sim U^2$  and thus control exponents only to order  $U/J$ . The discussed behavior is not restricted to the case of half filling. The inset of Fig. 3 shows  $|n_j^{\text{st}} - \nu|$  for  $\nu = 0.375$  on a log-log scale and the corresponding TL model prediction as the envelope.

To compute the steady-state linear conductance of the

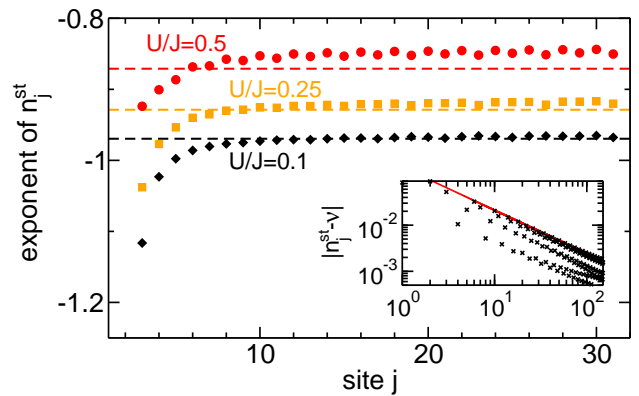


FIG. 3. (Color online) Functional RG data for the effective exponent of the Friedel oscillations of the steady-state density  $n_j^{\text{st}}$  for  $\nu = 1/2$ ,  $N = 10^3$ , and  $T = 0$  determined by taking the log-derivative. The predictions from the TL model with the exact lattice model  $K$  (dashed lines) are consistent with our results. The inset shows  $|n_j^{\text{st}} - \nu|$  at  $\nu = 0.375$  and  $U/J = 0.25$  (symbols). The line is the TL model prediction.

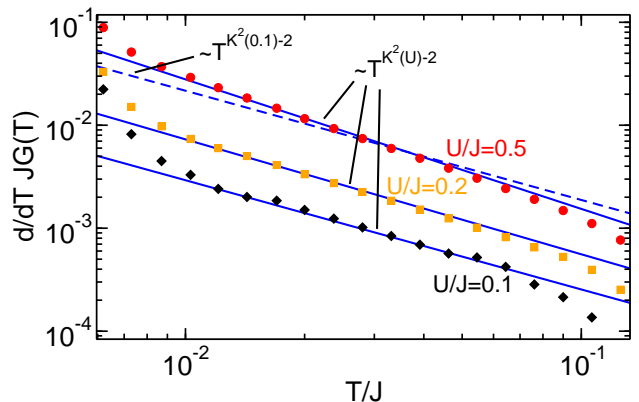


FIG. 4. (Color online) Functional RG data for the temperature derivative of the steady-state linear conductance of our lattice model for a weak impurity  $h/J = 0.05$ , filling  $\nu = 1/2$ , and  $N = 10^3$  (symbols). The prediction from the TL model with the exact lattice model  $K$  is shown as the solid lines. To emphasize the sizable differences in the exponents we have added a power law with the  $U/J = 0.1$  exponent as the dashed line to the  $U/J = 0.5$  data.

lattice model we take the canonical density matrix  $\rho_c^0$  (with  $T > 0$ ) corresponding to  $H_{\text{LM}}(U = 0) + H_{\text{imp}}$  as the initial state. The time evolution is performed with  $H_{\text{LM}}(U > 0) + H_{\text{imp}}$  supplemented by onsite energies  $V/2$  ( $-V/2$ ) for all  $j \leq N/2$  ( $j > N/2$ ). The current  $I(t)$  across the impurity bond is computed. Following the same reasoning as for the density  $I$  becomes stationary for  $t$  of the order of  $10^2/J$ . We take  $V$  to be the smallest energy scale of the problem (typically  $V = 10^{-3}J$ ) to ensure that we are in the linear regime  $I^{\text{st}} = GV$ . For  $T \gg J$  we find  $G(T) \sim T^{-1}$ ,<sup>13</sup> which is a band effect (see the inset of Fig. 5). The universal scaling of the conductance discussed in the last section can only be expected for  $T \ll J$ .

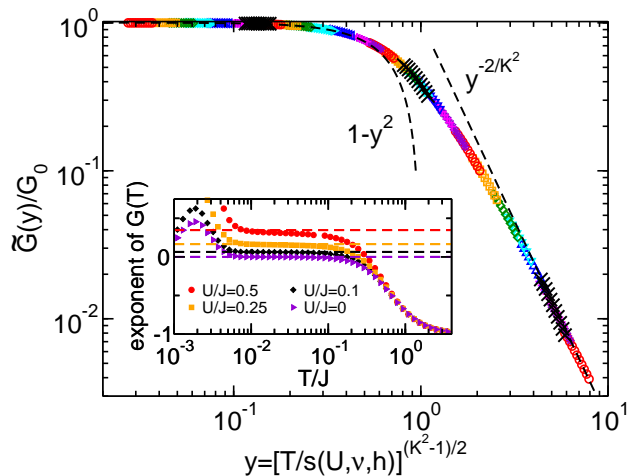


FIG. 5. (Color online) Functional RG data for the one-parameter scaling of  $\tilde{G}(y)$  of the lattice model for  $U/J = 0.5$ ,  $\nu = 1/2$ , and  $N = 10^3$ . Different symbols stand for different  $h$  increasing from left to right. No fixed point in between the perfect and the steady-state analog of the open chain ones exist. The crosses were computed for  $U/J = 0.85$ ,  $\nu = 1/4$  giving the same  $K$ . The scaling function thus depends on  $U$  and  $\nu$  only via  $K$ .<sup>11</sup> The prediction of the TL model for  $y \rightarrow 0$  and  $y \rightarrow \infty$  with the exact lattice model  $K$  is shown as dashed lines. Inset: the effective exponent of  $G(T)$  for a strong impurity  $h/J = 0.9$  determined by a log-derivative. Dashed lines show the prediction of the TL model with the exact lattice model  $K$ .

We first analyze the case of weak impurities. To eliminate the constant  $G_0$  we take the derivative of  $G$  with respect to  $T$ . Based on our above considerations we expect to find  $dG/dT \sim T^{K^2-2}$ ; see Fig. 4. Over roughly one order of magnitude the functional RG data follow the TL model prediction with the exact  $K$  of our lattice model. The deviations for  $T/J > 0.1$  indicate the crossover to the nonuniversal  $G(T) \sim T^{-1}$  regime. The ones for  $T/J < 0.01$  have two reasons. As discussed above the scaling only holds as long as  $T$  does not become too small. Furthermore, the energy level spacing  $\delta_N = v_F/N$  ( $= 2 \cdot 10^{-3}J$  for the parameters of the plot) is an energy scale of the problem which cuts off any universal behavior.<sup>12,13</sup> This is an artefact of our treatment of finite systems. For small  $h$  and  $T/J \in [0.1, 0.005]$ ,  $G_0 - G(T) \ll 1$ . Our analysis thus requires very accurate data. To minimize the error due to small residual oscillations of  $I(t)$  present even for  $t$  of the order of  $10^2/J$  we averaged the data at large  $t$  over a small time interval.

In the inset of Fig. 5 we present our results for  $G(T)$  across a strong impurity. Even without any  $t$  averaging our data are accurate enough such that the log-derivative, that is the effective exponent, gives a smooth curve. The data clearly show the crossover from the nonuniversal  $T^{-1}$  behavior at large  $T$  to the TL model prediction  $T^{K^2-1}$  at low ones. For  $T \rightarrow 0$  the scaling is cut off by both the finite size scale  $\delta_N$  as well as the finite DOS at  $\omega = 0$  [see Eq. (5)]. In the limits of strong and weak

impurities our results for the linear conductance of the lattice model thus agree to the TL model prediction providing the second indication of LL universality of the steady state.

We finally show that in the steady state of the lattice model no fixed point in between the perfect and the steady-state analog of the open chain ones exist. To this end we compute  $G(T)$  for a variety of  $h$  at fixed  $U$  and  $\nu$ . Using a one-parameter scaling ansatz of the form  $G(T) = \tilde{G}(y)$ ,<sup>11,13</sup> with  $y = (T/s)^{(K^2-1)/2}$  and the nonuniversal scale  $s(U, \nu, h)$ , all data can be collapsed on a single curve continuously connecting the weak ( $y \rightarrow 0$ ) and strong ( $y \rightarrow \infty$ ) impurity fixed points; see the main plot of Fig. 5.

#### IV. OPEN QUESTIONS

We provided evidence that the steady state of an interacting 1d lattice model after a quantum quench shows LL universality. Our analysis relies on the functional RG approach in its lowest-order truncation,<sup>25,26</sup> which is sufficient to obtain LL power laws with  $U$ -dependent exponents. An obvious first question arising is if higher order terms in  $U/J$  might change this picture. In fact, a series of RG studies of the field-theoretical TL model complemented by ‘perturbations’ indicates, that power-law scaling is destroyed on long times by certain such terms.<sup>20–22</sup> In nonequilibrium it is not established if and how the field theory studied in those papers is related to microscopic lattice models considered by us.<sup>44</sup> Currently, the results of Refs. 20–22 and our findings should thus be viewed as complementary and not contradicting. We emphasize that the notion of LL universality involves lattice models and not only field theories.<sup>8</sup> The numerically ‘exact’ results of Ref. 23 for the time-evolution towards the steady state are consistent with our findings. For the  $U/J \leq 0.5$  considered by us the corrections of order  $(U/J)^2$  are small. Even if they would destroy the LL scaling on very large time scales, we expect that remnants of the predicted LL steady state can be found up to this scale. The second apparent open question is if and how the picture changes if a lattice model is considered which is not Bethe ansatz solvable (‘nonintegrable’). We here merely note that for the time dependence indications of universal LL power laws were found even for such models.<sup>23</sup>

#### ACKNOWLEDGMENTS

We thank S. Andergassen, E. Dalla Torre, C. Karrasch, A. Mitra, K. Schönhammer, D. Schuricht, and G. Uhrig for discussions as well as S. Blügel and the Jülich Supercomputing Centre for access to the JuDGE GPU cluster. This work was supported by the DFG via FOR 723.

## Appendix A: Bosonization

To compute observables and correlation functions in the steady state of the TL model with open boundaries after an interaction quench we use ‘open boundary bosonization’ for the Hamiltonian and the field operator.<sup>34–36,45</sup> We are interested in the scaling behavior with all energy scales send to zero and all length scales send to infinity. Thus subtleties resulting out of the momentum dependence of the two-particle potential  $u(k)$  become irrelevant<sup>19,46</sup> and the ultraviolet regularization can be implemented at will. To illustrate the procedure we consider the density  $n_t(x)$ . We first study the quench from  $u_i(k) = 0$  to  $u_f(k) = u(k)$ . For simplicity we focus on temperature  $T = 0$ . The density is given by the Green function

$$iG_t(x, x) = \langle \text{vac}(b) | e^{iH_{\text{TL}}t} \psi^\dagger(x) \psi(x) e^{-iH_{\text{TL}}t} | \text{vac}(b) \rangle,$$

with the noninteracting ground state  $|\text{vac}(b)\rangle$  which corresponds to the vacuum with respect to the  $b$ 's [see Eq. (1)]. The fields  $\psi^{(\dagger)}(x)$  contain the open boundary conditions. Using auxiliary fields  $\tilde{\psi}^{(\dagger)}(x)$  which are identical to the ones obtained for periodic boundary conditions<sup>6,7,24</sup> and are e.g. given in Eqs. (18)–(20) of Ref. 19, the Green function reads

$$\begin{aligned} iG_t(x, x) = & \frac{1}{2} \left[ \langle \text{vac}(b) | e^{iH_{\text{TL}}t} \tilde{\psi}^\dagger(x) \tilde{\psi}(x) e^{-iH_{\text{TL}}t} | \text{vac}(b) \rangle \right. \\ & + \langle \text{vac}(b) | e^{iH_{\text{TL}}t} \tilde{\psi}^\dagger(-x) \tilde{\psi}(-x) e^{-iH_{\text{TL}}t} | \text{vac}(b) \rangle \\ & - \langle \text{vac}(b) | e^{iH_{\text{TL}}t} \tilde{\psi}^\dagger(x) \tilde{\psi}(-x) e^{-iH_{\text{TL}}t} | \text{vac}(b) \rangle \\ & \left. - \langle \text{vac}(b) | e^{iH_{\text{TL}}t} \tilde{\psi}^\dagger(-x) \tilde{\psi}(x) e^{-iH_{\text{TL}}t} | \text{vac}(b) \rangle \right]. \end{aligned}$$

Those expectation values can be computed following the usual steps<sup>6,7,24</sup> which involve the multiple use of the Bogoliubov transformation  $b_n = c(k_n)\alpha_n + s(k_n)\alpha_n^\dagger$  and the Baker-Campbell-Hausdorff relation. The coefficients  $c(k_n)$  and  $s(k_n)$  depend on the two-particle potential  $u(k_n)$  and are e.g. given in Eq. (9) of Ref. 19. The first two terms of the Green function provide the homogeneous background density while the latter two oscillate in space with frequency  $2k_F$ —they contain the Friedel oscillations induced by the boundaries. After taking the thermodynamic limit and the limit  $t \rightarrow \infty$  we find for the steady-state access density

$$\Delta n^{\text{st}}(x) \sim x^{-[c^2(0)+s^2(0)][c(0)+s(0)]} \cos(2k_F x). \quad (\text{A1})$$

At zero momentum the coefficients of the Bogoliubov transformation can be expressed in terms of the models LL parameter  $K$  given in the main text as

$$s^2(0) = \frac{1}{4}(K + K^{-1} - 2), \quad c^2(0) = \frac{1}{4}(K + K^{-1} + 2) \quad (\text{A2})$$

Using those relations the exponent of Eq. (A1) can be written as  $-(K^2 + 1)/2$  (see Table I of the main text). The other scaling exponents of the last column of Table I of the main text can be obtained in a similar fashion.

In any (equilibrium) LL the LL parameter is given by

$$K = 1 - \tilde{U} + \mathcal{O}(\tilde{U}^2), \quad (\text{A3})$$

where  $\tilde{U}$  is a dimensionless measure for the interaction strength; e.g.  $\tilde{U} = u(0)/(2\pi v_F)$  for the TL model and  $\tilde{U} = U[1 - \cos(2k_F)]/[2\pi J \sin(k_F)]$  for our lattice model at filling  $\nu = k_F/\pi$ . Using this expansion it is evident that all scaling exponents discussed by us (see Table I of the main text) have a leading order contribution in  $\tilde{U}$ . This is crucial as within our approximate treatment of the lattice model we control exponents only to leading order.<sup>25</sup>

We next briefly discuss the case when starting in the ground state of  $H_{\text{TL}}$  with  $u_i(k) > 0$  and performing the time evolution with a different interaction  $u_f(k) > 0$ ; all quantities depending on the interaction strength acquire indices  $i$  or  $f$ . We have to consider two Bogoliubov transformations [corresponding to the transformations from zero interaction to  $u_{i/f}(k)$ ] and two sets of eigenmode ladder operators. The initial state is the vacuum with respect to one of those while the Hamiltonian with which the time evolution is performed is a diagonal quadratic form in the other one. Repeatedly applying the Bogoliubov transformations and the Baker-Campbell-Hausdorff relation gives for the steady-state access density

$$\Delta n^{\text{st}}(x) \sim x^{-\gamma} \cos(2k_F x), \quad (\text{A4})$$

with the scaling exponent

$$\begin{aligned} \gamma = K_f \left[ 1 + \frac{1}{8}(K_i + K_i^{-1} - 2)(K_f + K_f^{-1} + 2) \right. \\ \left. - \frac{1}{4}(K_i - K_i^{-1})(K_f - K_f^{-1}) \right. \\ \left. + \frac{1}{8}(K_i + K_i^{-1} + 2)(K_f + K_f^{-1} - 2) \right]. \quad (\text{A5}) \end{aligned}$$

For  $K_i = 1$ , that is if we start in the noninteracting ground state, it becomes equal to  $(K_f^2 + 1)/2$  (see Table I of the main text). Using the expansion Eq. (A3) it is easy to see that  $\gamma$  and  $(K_f^2 + 1)/2$  agree to leading order in the two-particle interaction, that is  $U_i$  only contributes to order  $U_i^2$  and  $U_f U_i$  or higher. To leading order in the interaction strength the scaling exponent of the density is thus exclusively given by  $U_f$ . The same holds for the other exponents considered by us (see Table I of the main text). In our computations for the lattice model we control exponents only to leading order which explains why in the main text we exclusively consider quenches out of the noninteracting ground state.

## Appendix B: Numerical implementation of the functional RG

We can calculate  $G^{K,\Lambda}(t, t')$  very efficiently by using an iterative procedure. First, we discretize time in steps such that during one small step  $\Delta t$  the time dependent

self-energy can be set constant. For our results shown in the main text we made sure that  $\Delta t$  is always chosen small enough such that further reducing it does not lead to any changes visible on the scale of the respective plots. We use

$$G^{\text{ret},\Lambda}(t, t')G^{\text{ret},\Lambda}(t', t'') \\ = -i\Theta(t - t')\Theta(t' - t'')G^{\text{ret},\Lambda}(t, t''). \quad (\text{B1})$$

$$G^{\text{ret},\Lambda}(t, t') = [G^{\text{adv},\Lambda}(t', t)]^\dagger, \quad (\text{B2})$$

to write  $G^{\text{ret}}(t, t')$  as a product of Green functions<sup>26</sup>

$$G^{\text{ret},\Lambda}(t_1 + \Delta t, t_1) = -ie^{-i[\epsilon + \bar{\Sigma}^{\text{ret},\Lambda}(t_1)]\Delta t}e^{-i\Lambda(t-t')}, \quad (\text{B3})$$

where  $\bar{\Sigma}^{\text{ret},\Lambda}(t_1)$  is the self-energy time averaged over the interval  $(t_1, t_1 + \Delta t)$ . The interacting Keldysh Green function  $G^{\text{K},\Lambda}(t, t)$  can then be found iteratively employing

$$G^{\text{K},\Lambda}(t + \Delta t, t + \Delta t) \\ = G^{\text{ret},\Lambda}(t + \Delta t, t)G^{\text{K},\Lambda}(t, t)G^{\text{ret},\Lambda}(t, t + \Delta t), \quad (\text{B4})$$

$$G^{\text{K},\Lambda}(0, 0) = -i(1 - 2\bar{n}). \quad (\text{B5})$$

In every time step two matrix exponentials of  $N \times N$  matrices have to be performed and multiplied with the Keldysh component of the Green function of the previous one. This renders the problem a natural candidate for graphics processing unit (GPU) supported algorithms. We use such to compute the results shown in the main text. The number  $N_t$  of time steps needed to obtain sufficient accuracy (and resolution) as well as to reach times which are large enough such that the physics is dominated by the steady state enters the number of equations to be solve. For the Hamiltonian considered in the main text we solve sets of  $(3N - 2)N_t$  coupled differential equations. Due to the nearest neighbor structure of the interaction  $3N - 2$  components of the self energy flow for each of the  $N_t$  time steps. Typical numbers considered are  $N = 1000$  lattice sites and  $N_t = 1600$  time steps.

- 
- <sup>1</sup> I. Bloch, J. Dalibard, and W. Zwerger, *Rev. Mod. Phys.* **80**, 885 (2008).  
<sup>2</sup> A. Polkovnikov, K. Sengupta, A. Silva, and M. Vengalattore, *Rev. Mod. Phys.* **83**, 863 (2011).  
<sup>3</sup> M. Rigol, V. Dunjko, V. Yurovsky, and M. Olshanii, *Phys. Rev. Lett.* **98**, 050405 (2007).  
<sup>4</sup> T. Barthel and U. Schollwöck, *Phys. Rev. Lett.* **100**, 100601 (2008).  
<sup>5</sup> M. Fagotti and F.H.L. Essler, *Phys. Rev. B* **87**, 245107 (2013).  
<sup>6</sup> T. Giamarchi, *Quantum Physics in One Dimension* (New York: Oxford University Press, 2003).  
<sup>7</sup> K. Schönhammer in *Interacting Electrons in Low Dimensions* ed. by D. Baeriswyl (Dordrecht: Kluwer Academic Publishers, 2005).  
<sup>8</sup> F.D.M. Haldane, *Phys. Rev. Lett.* **45**, 1358 (1980).  
<sup>9</sup> J. Sólyom, *Adv. Phys.* **28**, 201 (1979).  
<sup>10</sup> A. Luther and I. Peschel, *Phys. Rev. B* **9**, 2911 (1974).  
<sup>11</sup> C.L. Kane and M.P.A. Fisher, *Phys. Rev. Lett.* **68**, 1220 (1992).  
<sup>12</sup> S. Andergassen, T. Enss, V. Meden, W. Metzner, U. Schollwöck, and K. Schönhammer, *Phys. Rev. B* **70**, 075102 (2004).  
<sup>13</sup> T. Enss, V. Meden, S. Andergassen, X. Barnabe-Therault, W. Metzner, and K. Schönhammer, *Phys. Rev. B* **71**, 155401 (2005).  
<sup>14</sup> M.A. Cazalilla, *Phys. Rev. Lett.* **97**, 156403 (2006).  
<sup>15</sup> G.S. Uhrig, *Phys. Rev. A* **80**, 061602 (2009).  
<sup>16</sup> A. Iucci and M.A. Cazalilla, *Phys. Rev. A* **80**, 063619 (2009).  
<sup>17</sup> D.M. Kennes and V. Meden, *Phys. Rev. B* **82**, 085109 (2010).  
<sup>18</sup> B. Dóra, M. Haque, and G. Zaránd, *Phys. Rev. Lett.* **106**, 156406 (2011).  
<sup>19</sup> J. Rentrop, D. Schuricht, and V. Meden, *New J. Phys.* **14**, 075001 (2012).  
<sup>20</sup> A. Mitra and T. Giamarchi, *Phys. Rev. Lett.* **107**, 150602 (2011).  
<sup>21</sup> A. Mitra and T. Giamarchi, *Phys. Rev. B* **85**, 075117 (2012).  
<sup>22</sup> A. Mitra, *Phys. Rev. B* **87**, 205109 (2013).  
<sup>23</sup> C. Karrasch, J. Rentrop, D. Schuricht, and V. Meden, *Phys. Rev. Lett.* **109**, 126406 (2012).  
<sup>24</sup> J. von Delft and H. Schoeller, *Annalen der Physik* **7**, 225 (1998).  
<sup>25</sup> W. Metzner, M. Salmhofer, C. Honerkamp, V. Meden, and K. Schönhammer, *Rev. Mod. Phys.* **84**, 299 (2012).  
<sup>26</sup> D.M. Kennes, S.G. Jakobs, C. Karrasch, and V. Meden, *Phys. Rev. B* **85**, 085113 (2012).  
<sup>27</sup> U. Schollwöck, *Ann. Phys.* **326**, 96 (2011).  
<sup>28</sup> G. Vidal, *Phys. Rev. Lett.* **93**, 040502 (2004).  
<sup>29</sup> S. R. White and A. E. Feiguin, *Phys. Rev. Lett.* **93**, 076401 (2004).  
<sup>30</sup> A. Daley, C. Kollath, U. Schollwöck, and G. Vidal, *J. Stat. Mech.*, P04005 (2004).  
<sup>31</sup> S.A. Hamerla and G.S. Uhrig, *New J. Phys.* **15**, 073012 (2013).  
<sup>32</sup> F. Pollmann, M. Haque, and B. Dóra, *Phys. Rev. B* **87**, 041109(R) (2013).  
<sup>33</sup> B. Dóra, F. Pollmann, J. Fortágh, and G. Zaránd, *Phys. Rev. Lett.* **111**, 046402 (2013).  
<sup>34</sup> M. Fabrizio and A.O. Gogolin, *Phys. Rev. B* **51**, 17827 (1995).



- <sup>35</sup> A.E. Mattsson, S. Eggert, and H. Johannesson, Phys. Rev. B **56**, 15615 (1997).
- <sup>36</sup> V. Meden, W. Metzner, U. Schollwöck, O. Schneider, T. Stauber, and K. Schönhammer, Eur. Phys. J. B **16**, 631 (2000).
- <sup>37</sup> F.H.L. Essler, S. Evangelisti, and M. Fagotti, Phys. Rev. Lett. **109**, 247206 (2012).
- <sup>38</sup> C. Klöckner, D.M. Kennes, and V. Meden, in preparation.
- <sup>39</sup> J. Rammer, *Quantum Field Theory of Non-equilibrium States* (Cambridge University Press, Cambridge, 2007).
- <sup>40</sup> Y. Meir and N.S. Wingreen, Phys. Rev. Lett. **68**, 2512 (1992).
- <sup>41</sup> P. Calabrese and J. Cardy, J. Stat. Mech. P10004 (2007).
- <sup>42</sup> S. Langer, F. Heidrich-Meisner, J. Gemmer, I.P. McCulloch, and U. Schollwöck, Phys. Rev. B **79**, 214409 (2009).
- <sup>43</sup> M. Ganahl, E. Rabel, F.H.L. Essler, and H.G. Evertz, Phys. Rev. Lett. **108**, 077206 (2012).
- <sup>44</sup> A. Mitra, private communication.
- <sup>45</sup> S. Grap and V. Meden, Phys. Rev. B **80**, 193106 (2009).
- <sup>46</sup> V. Meden, Phys. Rev. B **60**, 4571 (1999).